ACS OMEGA

Article

http://pubs.acs.org/journal/acsodf

Nano-Heteroarchitectures of Two-Dimensional MoS_2@ One-Dimensional Brookite TiO_2 Nanorods: Prominent Electron Emitters for Displays

Rupesh S. Devan,*[,†] Vishal P. Thakare,[‡] Vivek V. Antad,[‡,§] Parameshwar R. Chikate,[†] Ruchita T. Khare,[∥] Mahendra A. More,[∥] Rajendra S. Dhayal,[⊥] Shankar I. Patil,[∥] Yuan-Ron Ma,[#] and Lukas Schmidt-Mende[▽]

[†]Discipline of Metallurgy Engineering & Materials Science, Indian Institute of Technology Indore, Simrol, Indore 453552, India
[‡]Physical & Materials Chemistry Division, CSIR-National Chemical Laboratory, Dr. Homi Bhabha Road, Pune 411008, India
[§]Nowrosjee Wadia College of Arts and Science, 19, Late Prin. V. K. Joag Path, Pune 411001, India
[∥]Department of Physics, Savitribai Phule Pune University, (Formerly, University of Pune), Pune 411007, India
[⊥]Centre for Chemical Sciences, School of Basics and Applied Sciences, Central University of Punjab, Bathinda 151001, India
[#]Department of Physics, National Dong Hwa University, Hualien 97401, Taiwan, R.O.C.
[▽]Department of Physics, University of Konstanz, Constance 78457, Germany

Supporting Information

ABSTRACT: We report comparative field electron emission (FE) studies on a large-area array of two-dimensional MoS_2-coated @ one-dimensional (1D) brookite (β) TiO_2 nanorods synthesized on Si substrate utilizing hot-filament metal vapor deposition technique and pulsed laser deposition method, independently. The 10 nm wide and 760 nm long 1D β-TiO_2 nanorods were coated with MoS_2 layers of thickness ~4 (±2), 20 (±3), and 40 (±3) nm. The turn-on field (E_{on}) of 2.5 V/μm required to a draw current density of 10 $\mu A/cm^2$ observed for MoS_2-coated 1D β-TiO_2 nanorods emitters is significantly lower than that of doped/undoped 1D TiO_2 nanostructures, pristine MoS_2 sheets, MoS_2@SnO_2, and TiO_2@MoS_2 heterostructure-based field emitters. The orthodoxy test confirms the viability of the field emission measurements, specifically field enhancement factor (β_{FE}) of the MoS_2@TiO_2/Si emitters. The enhanced FE behavior of the MoS_2@TiO_2/Si emitter can be attributed to the modulation of the electronic properties due to heterostructure and interface effects, in addition to the high aspect ratio of the vertically aligned TiO_2 nanorods. Furthermore, these MoS_2@TiO_2/Si emitters exhibit better emission stability. The results obtained herein suggest that the heteroarchitecture of MoS_2@β-TiO_2 nanorods holds the potential for their applications in FE-based nanoelectronic devices such as displays and electron sources. Moreover, the strategy employed here to enhance the FE behavior via rational design of heteroarchitecture structure can be further extended to improve other functionalities of various nanomaterials.

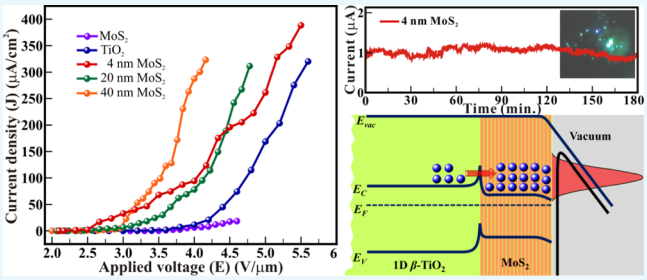

INTRODUCTION

The high aspect ratio and sharp tip features of one-dimensional (1D) metal oxide nanostructures have engaged most of the researchers to explore their electronic/physical properties for the development of efficient functional devices for energy conversion and conservation.[1−4] TiO_2 is one of them, but it is explored to a certain extent for field emission displays despite its low work function of 3.9−4.5 eV.[5] The nanotubular geometric analogy of TiO_2 with the carbon nanotubes have engrossed researcher to investigate their field electron emission (FE) behaviors.[5−8] Moreover, dissimilar distortion of TiO_6 octahedra produced the crystalline structures of rutile, anatase, and brookite crystalline phases. Nevertheless, exploration of limited 1D morphologies of TiO_2, random dispersion of TiO_2 1D nanostructures, and electron field screening effect have adverse affect on their further FE studies.[1,9,10] Thermodynamically most stable β-phase at dimensions of 11−35 nm[11] needs to be explored to overcome the field screening effect by providing homogeneous 1D nanostructures.[12] Even though N, Fe, and C were doped to enhance the FE characteristics of 1D TiO_2 nanostructures,[6,13,14] the heterostructures of TiO_2 with other metal oxides or conducting materials need to be adopted for further improving the FE performance for industrial/scientific applications. Recently, various conducting two-dimensional (2D) materials, including C,[14] MoS_2,[15−17] and WS_2,[15] have been introduced as coatings over metal oxides and vice verse, utilizing complex chemical/physical processes to produce heterostructures. The metal oxide nanostructures

Received: March 23, 2017
Accepted: June 8, 2017
Published: June 23, 2017

DOI: 10.1021/acsomega.7b00345
ACS Omega 2017, 2, 2925−2934

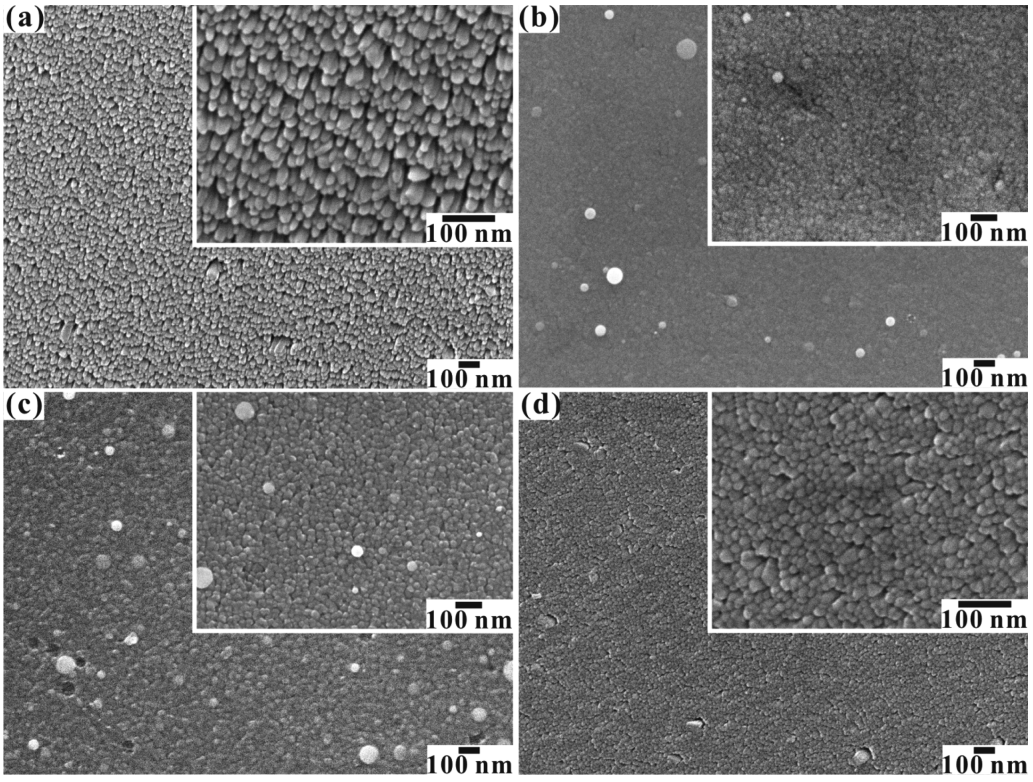

Figure 1. FESEM images showing the top view of the large-area array of (a) vertically aligned pristine 1D β-TiO_2 nanorods on Si substrate, which were further decorated with (b) 40 nm, (c) 20 nm, and (d) 4 nm layer/shell of MoS_2. The inset shows their respective high-magnification FESEM images.

coupled or modified with a coating to form layered or core−shell structures have shown significant improvement in their properties and applications in photocatalysis,[15] decompositions of organic dyes,[16] and batteries.[17] Among these coating materials, MoS_2, a transitional metal dichalcogenide with a layered 2D planar structure similar to that of graphene and a narrow band gap of 1.7 eV (in the bulk form), is one of the most promising coating materials.[18] Recent report confirms that MoS_2 appears to be a good field emitter because of its unique electronic properties.[19] Therefore, the improvement in the FE performance should be feasible with shell formation of 2D materials over 1D metal oxide nanostructures. MoS_2 nanoflowers and clusters decorated with ZnO[20] and SnO_2[21] nanoparticles delivered a turn-on field of 3.08 and 3.4 V/μm, respectively. The field emitter of amorphous carbon nanocone shells on TiO_2 nanowire cores has provided the turn-on field of 3.1 V/μm.[22] Recently, Fu et al.[23] have reported FE properties of rutile TiO_2 hierarchical network heavily loaded with MoS_2. However, the FE properties were not optimized for controlled growth of MoS_2 layers, and highly dense TiO_2 nanorods arranged in the form of dandelion flowerlike morphology were seldom covered with MoS_2. Moreover, morphology characterized by randomly oriented 1D nanostructures of high areal density suffers from significant field screening effect, thereby exhibiting poorer FE behavior. Furthermore, randomly distributed anatase TiO_2 nanorods covered with dense MoS_2 thin film provided the turn-on field of 11 V/μm,[24] which is very high compared to pure TiO_2 nanostructures and MoS_2 layers reported in the literature. Consequently, for promising FE behavior, it is of scientific and technological importance to grow vertically aligned 1D β-TiO_2 nanorods and furthermore tailor their electronic properties via the formation of heterostructure with an ultrathin 2D MoS_2 layer.

In this work, we present 1D β-TiO_2 nanorods/2D MoS_2 layered and core−shell nanostructure arrays as excellent field emitters. The large-area arrays of vertically aligned TiO_2 nanorods of brookite phase were synthesized using hot-filament metal vapor deposition (HF-MVD) technique, which is a unique and simple method to provide diverse morphologies and crystalline structures of various metal oxide nanostructures.[25−30] Furthermore, MoS_2 layers/shell of desired thicknesses were grown over β-TiO_2 nanorods utilizing the pulsed laser deposition (PLD) technique, which is one of the advanced, versatile technologies used for growing layered/shell materials with excellent adhesion, perfect stoichiometric growth, and better scalability to smaller geometries.[31−34] The influence of MoS_2 layer thickness on the structural, chemical, and FE characteristics was studied. The structural morphology, electronic structure, and chemical composition of MoS_2-coated β-TiO_2 nanorods were examined utilizing X-ray photoemission spectroscopy (XPS) and field-emission scanning electron microscopy (FESEM). The comparative FE studies of MoS_2-coated β-TiO_2 nanorods were performed after the optimization of anode−cathode separations for pure β-TiO_2 nanorods. The MoS_2@β-TiO_2 nanorod heteroarchitectures with ∼4 nm MoS_2 shell thickness exhibited excellent FE properties.

RESULTS AND DISCUSSION

The FESEM images in Figure 1 show the surface morphology of pure TiO_2 nanorods and MoS_2-loaded TiO_2 nanorods synthesized on Si substrate. The top view of a portion of the array in Figure 1a shows a uniform distribution of TiO_2 nanorods over a large area. The vertically aligned TiO_2

DOI: 10.1021/acsomega.7b00345
ACS Omega 2017, 2, 2925−2934

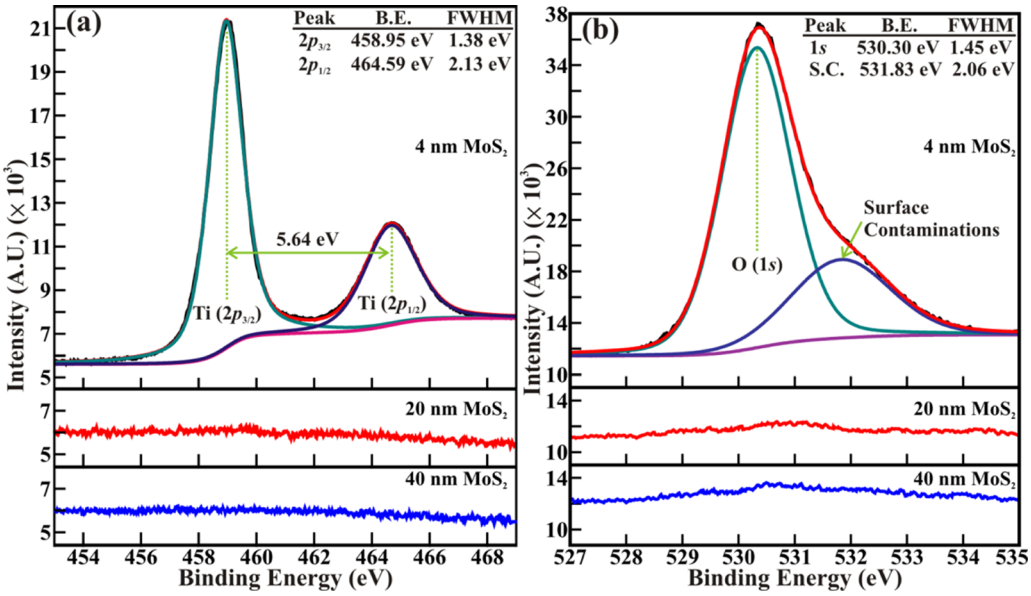

Figure 2. High-resolution XPS spectra of (a) Ti(2p) and (b) O(1s) core levels of the large-area array of 2D MoS_2@1D β-TiO_2 nanorods with 40 nm (lower panel), 20 nm (middle panel), and 4 nm (upper panel) layer/shell of MoS_2. The XPS spectra are decomposed via Voigt curve function fitting.

nanorods of the average diameter of ∼10 nm were well separated with their clearly visible textural boundaries (inset of Figure 1a). More details on the surface morphological feature of pure TiO_2 nanorods are explained elsewhere.[12] These as-synthesized 1D TiO_2 nanorods were exclusively composed of orthorhombic crystals in brookite (β) phase assigned to the space group *Pbca* (JCPDS − 761936) with lattice constants a = 0.919 nm, b = 0.546 nm, c = 0.516 nm, and $\alpha = \beta = \gamma = 90°$. Further, selected area electron diffraction pattern of nanorods indexed to the [101] zone axis corroborates the formation of brookite (β)-TiO_2 nanorods. A detailed explanation of the crystalline structure of TiO_2 nanorods is provided elsewhere.[12] After the formation of β-TiO_2 nanorods array over a large area was confirmed, these vertically aligned β-TiO_2 nanorods were subjected to controlled growth of MoS_2 layers over the surface of nanorod body, utilizing the PLD technique. The growth of thin layers of MoS_2 over the β-TiO_2 nanorods was controlled by monitoring the deposition rates at an optimized laser energy density. FESEM images in Figure 1b,c show the surface morphologies of the MoS_2-loaded β-TiO_2 nanorods. A close examination of the top view of a portion of array shows that the entire β-TiO_2 nanorods array is uniformly covered with MoS_2 layers. The MoS_2 layers of an average thickness of ∼40 (±3 nm), ∼20 (±3 nm), and ∼4 (±2 nm) nm were synthesized at optimized deposition rates. Details of the single-crystalline MoS_2 formation and their thickness variations are provided in Supporting Information. Figure 1b shows the FESEM image of MoS_2 thin film over β-TiO_2 nanorods array synthesized at an optimized deposition rate of ∼1000 shots. The uniform thin film of ∼40 nm thick MoS_2 was produced over a large-area array of β-TiO_2 nanorods. The high-magnification FESEM image in the inset of Figure 1b shows that MoS_2 forms a nonporous thin film of uniform thickness to cover the entire β-TiO_2 nanorods array, and no β-TiO_2 nanorods are visible at all. Further, the thickness of MoS_2 layer on β-TiO_2 nanorods was reduced to ∼20 nm (Figure 1c) by decreasing the deposition rate (∼500 shots). The high-magnification FESEM image in the inset of Figure 1c shows a kind of growth of nanoparticles of MoS_2 over β-TiO_2 nanorods array. However, they are not MoS_2 nanoparticles in particular. The growth of MoS_2 layers continued distinctly over the top of β-TiO_2 nanorods to deliver nanoparticles like morphological look, which resulted in a larger surface roughness than that of MoS_2 layers of ∼40 nm thickness over β-TiO_2. The increase in the surface area because of the roughness is expected to contribute positively to the FE behavior. The deposition was reduced further to grow only a few layers of MoS_2 on vertically aligned β-TiO_2 nanorods. The FESEM image in Figure 1d shows that very thin layer of MoS_2 was yielded (at ∼100 shots) on the large-area array of well-separated β-TiO_2 nanorods. The overgrowth or island formations of MoS_2 was not observed. The high-magnification FESEM image in the inset of Figure 1d shows that the β-TiO_2 nanorods were shelled with few layers of MoS_2 to form ∼4 nm thick layer. The MoS_2 shell might have covered all of the nanorods body. Therefore, the separation between MoS_2-coated β-TiO_2 nanorods (Figure 1d) was less than that between the as-deposited β-TiO_2 nanorods (Figure 1a). Nevertheless, TiO_2@MoS_2 core−shell nanorods were well separated from each other. At a thickness of ∼4 nm, 6−7 layers of MoS_2 are expected to be present based on the previously reported thickness of 0.7 nm for a monolayer of S−Mo−S (i.e., MoS_2) structure.[35] This confirms that MoS_2 shell of ∼4 nm thickness on the core of β-TiO_2 nanorods is converted further into thin films of thickness ∼20 and ∼40 nm.

Independent XPS studies were performed to investigate the electronic structure and chemical properties of β-TiO_2 nanorods and MoS_2@β-TiO_2 nanorods. Figure 2 illustrates the high-resolution XPS spectra for Ti(2p) and O(1s) recorded after the growth of thin MoS_2 layers of thickness ∼4, ∼20, and ∼40 nm on β-TiO_2 nanorods. The middle and lower panels of Figure 2a,b show that the intensity of Ti(2p) and O(1s) is almost zero (invariable). The formation of MoS_2 of thickness ∼20 and ∼40 nm on β-TiO_2 nanorods resulted in the disappearance of Ti(2p) and O(1s) peaks because of the allowed fine-depth profiling only within 10 nm in XPS. The absence of O(1s) peak implies that neither suboxide/oxidized phases of Mo nor additional oxides were formed along with MoS_2 on the β-TiO_2 nanorods. On the other hand, distinct

DOI: 10.1021/acsomega.7b00345
ACS Omega 2017, 2, 2925−2934

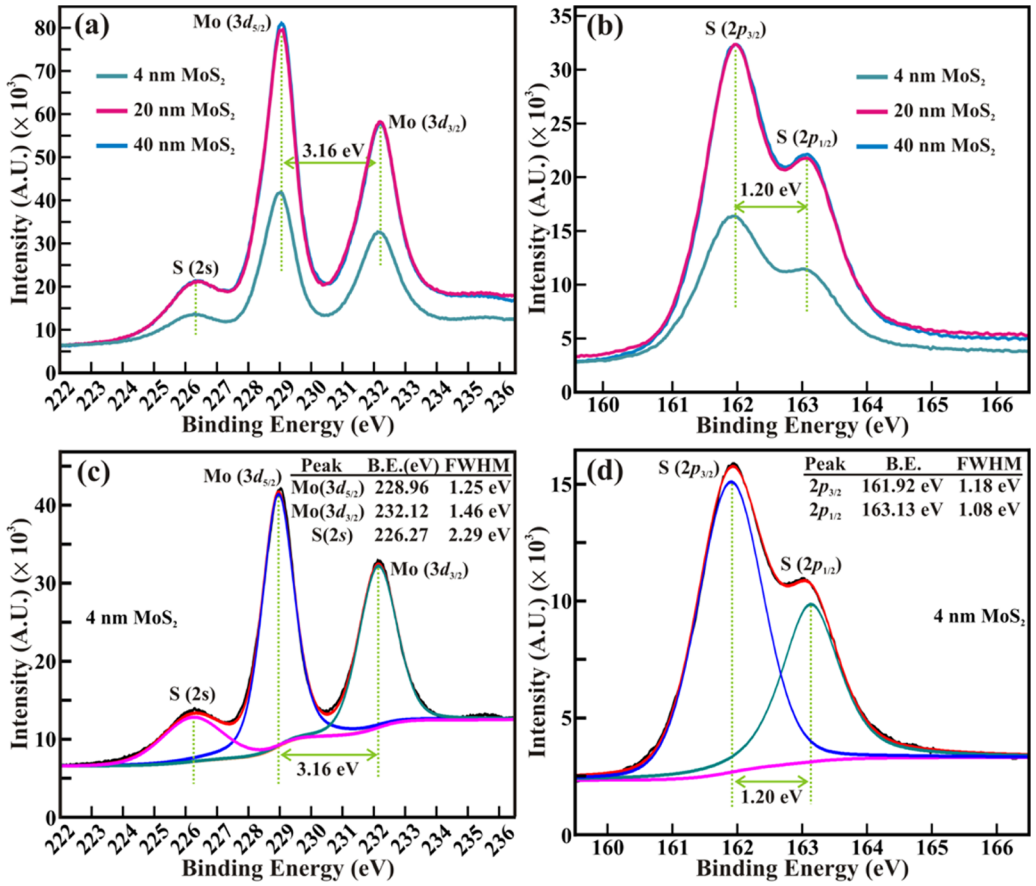

Figure 3. Typical high-resolution XPS spectra of (a) Mo(3d) and (b) S(2p) core levels of the 2D MoS_2@1D β-TiO_2 nanorods decorated with ∼40, 20, and 4 nm layer/shell of MoS_2. The deconvoluted XPS spectra of (c) Mo(3d) and (d) S(2p) core levels of ∼4 nm thick MoS_2 shell loaded β-TiO_2 nanorods. The XPS spectra are deconvoluted via Voigt curve function fitting.

XPS peaks for Ti(2p) and O(1s) were observed for the β-TiO_2 nanorods array coated with MoS_2 of thickness ∼4 nm and are shown in the upper panel of Figure 2a,b, respectively. The Ti(2p) XPS spectra were deconvoluted via Voigt curve fitting function within the Shirley background (upper panel, Figure 2a) to determine the double peak features of Ti($2p_{3/2}$) and Ti($2p_{1/2}$) in particular. The perfect fit for two peaks located at the binding energies of 458.95 and 464.59 eV evidenced Ti($2p_{3/2}$) and Ti($2p_{1/2}$) core levels of Ti^{4+} cations only, respectively, and not of Ti^{3+} or other suboxides.[12,36,37] The Ti($2p_{3/2}$) and Ti($2p_{1/2}$) peaks with the energy separation of 5.64 eV and the full width at half-maximum (FWHM) of 1.38 and 2.13, respectively, are akin to that of pure β-TiO_2 nanorods.[12] Likewise, O(1s) XPS spectra of β-TiO_2 nanorods (upper panel, Figure 2b) were decomposed via Voigt curve fitting within the Shirley background, showing the perfect fits to two peaks located at the binding energies of 530.30 and 531.83 eV with FWHM of 1.45 and 2.06 eV, respectively. The lower binding energy peak observed at 530.30 eV corresponds to the O(1s) core level of the O^{2-} anions associated with the Ti−O chemical bonding (O_{1s}^{Ti-O})[12] in β-TiO_2 nanorods. However, higher binding peak at 531.83 eV is attributed to the nanorod surface contamination, such as carbon oxides or hydroxides.[12,38,39] Thus, the double peak features of the XPS spectra of Ti(2p) and O(1s) shown in Figure 2a (upper panel) and Figure 2b (upper panel), respectively, are akin to that of pure β-TiO_2 nanorods. The estimated atomic ratio (i.e., O/Ti ratio) of ∼1.99 (i.e., Ti/O = 1:1.99) of oxygen and titanium is very close to the stoichiometric ratio (i.e., 1:2) of pure TiO_2. These analyses are well consistent with that of the β-TiO_2 nanorods revealed earlier.[12] These results indicate that the loading of MoS_2 at laser energy density of 1 J/cm^2 did not alter the chemical and elemental properties β-TiO_2 nanorods.

Figure 3 illustrates Mo(3d) and S(2p) high-resolution XPS spectra of the MoS_2-loaded β-TiO_2 nanorods. Figure 3a,b confirms that the relative intensities of Mo(3d) and S(2p) peaks remain unaffected for MoS_2 of thickness ∼20 and ∼40 nm loaded on β-TiO_2 nanorods. The apparent change in their relative intensities was observed for ∼4 nm thick shell of MoS_2, as that has reflected in the appearance of intense peaks of Ti(2p) and O(1s) as shown in Figure 2. Which indicates that there was a significant expense in the intensities of Mo(3d) and S(2p) peaks and gain in the intensity of Ti(2p) and O(1s) peaks at ∼4 nm thick MoS_2 shell than that of ∼20 and ∼40 nm thick films. Thus, the change in the area under peaks reflect a variation in the thickness of MoS_2 to form a shell and thin film over β-TiO_2 nanorods. For precise determination of the peak features, XPS spectra were deconvoluted via Voigt curve fitting function. The deconvolution of Mo(3d) spectra of ∼4 nm thick MoS_2 shell loaded on β-TiO_2 nanorods in Figure 3c shows a perfect fit for three peaks. The peaks located at the binding energies of 228.96 and 232.12 eV, respectively, correspond to Mo($3p_{5/2}$) and Mo($3p_{3/2}$) core levels of the Mo^{4+} cations in MoS_2 and not of Mo^{6+}.[40−42] The shoulder peak near Mo($3p_{5/2}$) core level located at a binding energy of 226.27 eV was assigned to S(2s).[42,43] The energy separation between Mo($3p_{5/2}$) and

DOI: 10.1021/acsomega.7b00345
ACS Omega 2017, 2, 2925−2934

$Mo(3p_{3/2})$ peaks of 3.16 eV was (<3.3 eV) assigned to MoS_2.[42] The FWHM of $Mo(3p_{5/2})$ and $Mo(3p_{3/2})$ peaks were 1.25 and 1.46 eV, respectively. Similarly, deconvolution of S(2p) spectra of ∼4 nm thick MoS_2 shell loaded on β-TiO_2 nanorods in Figure 3d shows perfect fit to two peaks located at the binding energies of 161.92 and 163.13 eV, respectively, corresponding to the $S(2p_{3/2})$ and $S(2p_{1/2})$ core levels of S^{2-} of MoS_2.[43,44] The energy separation between $S(2p_{3/2})$ and $S(2p_{1/2})$ peaks of ≤1.4 was assigned to the formation of MoS_2 and that of ≥1.4 was assigned to amorphous MoS_3.[43,44] Therefore, the observed energy separation of 1.20 eV between $S(2p_{3/2})$ and $S(2p_{1/2})$ peaks reflects the formation of MoS_2 only and not of MoS_3 or any other compound. The FWHM of $S(2p_{3/2})$ and $S(2p_{1/2})$ peaks were 1.18 and 1.08 eV, respectively. Further, for precision determination of MoS_2 phase formation, the XPS spectra of ∼20 and ∼40 nm thick MoS_2 loaded on β-TiO_2 nanorods were decomposed (Figures S3 and S4). Irrespective of the change in the thickness of MoS_2 layers coated over β-TiO_2 nanorods, the $Mo(3p_{5/2})$, $Mo(3p_{3/2})$, $S(2p_{3/2})$, and $S(2p_{1/2})$ core levels were located at the binding energies of 228.97 (±0.01), 232.13 (±0.01), 161.93 (±0.01), and 163.13 (±0.01) eV, respectively. These peak positions were extremely identical to those observed in ∼4 nm MoS_2@TiO_2 nanorods, consequently corresponding to Mo^{4+} cations and S^{2-} anions, respectively. Moreover, distinct variation was not observed in the binding energy of S(2s) peak (i.e., 226.28 (±0.02) eV) appearing as a shoulder peak near $Mo(3p_{5/2})$ core level. The FWHM of $Mo(3p_{5/2})$ and $Mo(3p_{3/2})$ peaks were 1.21 and 1.39 (±0.02) for samples loaded with ∼20 and ∼40 nm thick layers of MoS_2, respectively. Similarly, the FWHM of $S(2p_{3/2})$ and $S(2p_{1/2})$ peaks were 1.06 and 1.04 (±0.01) eV, respectively. The relatively larger FWHM observed for ∼4 nm thick layers of MoS_2 compared with ∼20 and ∼40 nm thick layers can be correlated with their size reduction.[45] Even after increasing the thickness of MoS_2 up to ∼20 and ∼40 nm, the energy separation between the peaks of $Mo(3p_{5/2})$ and $Mo(3p_{3/2})$ (i.e., ∼3.16 (±0.01) eV) and $S(2p_{3/2})$ and $S(2p_{1/2})$ (i.e., ∼1.20 (±0.01) eV) remained akin to that of ∼4 nm thick MoS_2 layer. The estimated atomic ratio of molybdenum and sulfur (i.e., Mo/S ratio) for all of the thicknesses of MoS_2 is ∼0.49 (±0.005) (i.e., Mo/S = 1:2.04 (±0.02)), which is very close to the stoichiometric ratio (i.e., 1:2) of pure MoS_2. It substantiates that shells or thin layers formed on β-TiO_2 nanorod arrays were composed of pure stoichiometric MoS_2 only and not of MoS_3. Overall, the XPS investigation confirmed successful coating of MoS_2 in the form of shell (∼4 nm) and thin films of various thicknesses (∼20 and ∼40 nm) over large-area arrays of 1D β-TiO_2 nanorods without any alteration in the chemical properties of both MoS_2 and TiO_2.

The FE measurements of MoS_2-coated β-TiO_2 nanorods (≡2D MoS_2/1D β-TiO_2/Si) were performed in a planar diode configuration (the emission area of ∼0.30 cm^2) at optimized anode−cathode separation. Initially, the pristine β-TiO_2 nanorods (≡1D β-TiO_2/Si) were subjected to electron field emission at various separations of 500, 1000, 1500, and 2000 μm. The larger emission current density (i.e., ∼470 $\mu A/cm^2$), lower threshold field (E_{thr}) (i.e., 4.8 V/μm), and lowest turn-on field (E_{on}) (i.e., 3.9 V/μm) were observed at 2000 μm. A thorough explanation is available elsewhere.[12] Likewise, the pristine MoS_2 (≡2D MoS_2/Si) was also subjected to electron field emission at the separation of 1000, 1500, and 2000 μm (Figure S5). The larger emission current density of 30.4 $\mu A/cm^2$ (at 8.4 V/μm) and turn-on field (E_{on}) of 7.2 V/μm (at 10 $\mu A/cm^2$) were achieved for the anode−cathode separation of 1000 μm. The E_{on} values reduced from 7.2 to 4.3 V/μm with an increase in the anode−cathode separation from 1000 to 2000 μm. More detailed explanation of the field emission behavior of 2D MoS_2 is provided in Supporting Information. Owing to the exhibition of lower E_{on} for both 2D MoS_2/Si and β-TiO_2/Si, and delivery of larger emission current density of β-TiO_2/Si emitters at 2000 μm separation, the FE studies of MoS_2-coated β-TiO_2 nanorods (MoS_2/β-TiO_2/Si) were accomplished at same separation. The FE properties of β-TiO_2 nanorods coated with MoS_2 of various thicknesses are shown in Figure 4. The

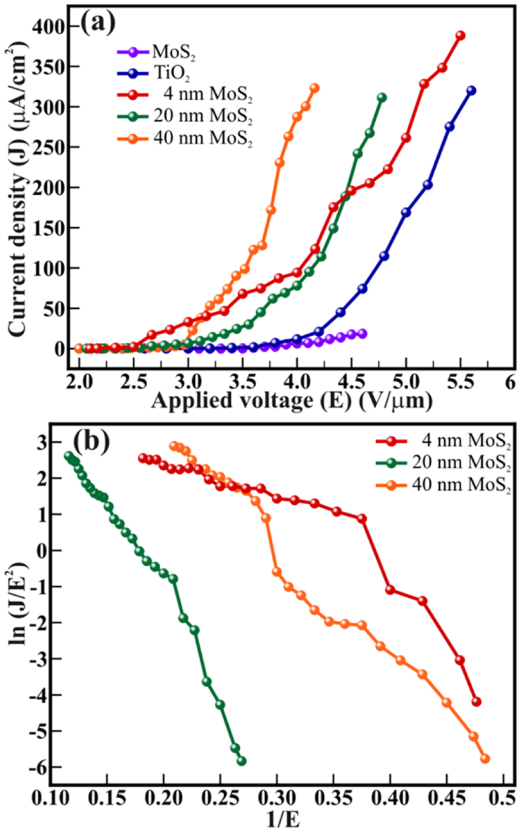

Figure 4. Field emission (a) J−E curves of a large-area array of vertically aligned pristine 1D β-TiO_2 nanorods, 2D MoS_2, and MoS_2@β-TiO_2 nanorods and MoS_2@β-TiO_2 nanorods decorated with ∼40, 20, and 4 nm layer/shell of MoS_2; and their corresponding (b) F−N plots measured at vacuum separations of 2000 μm.

applied electric field (E) dependent variation in the macroscopic electron emission current density (J) (i.e., J−E plot) of MoS_2/β-TiO_2/Si, β-TiO_2/Si, and MoS_2/Si emitters is shown in Figure 4a. A distinctive variation in the emission current was observed with the thickness of MoS_2. An applied electric field E ($=V/d_{sep}$) is in the form of the average field rather than uniform field between the electrodes separated by the distance d_{sep}. The MoS_2/β-TiO_2/Si emitters deliver larger emission current density at relatively lower applied fields compared with both β-TiO_2/Si and MoS_2/Si emitters. Especially, ∼4 nm thick shell of MoS_2 on β-TiO_2 nanorods yields a larger emission current density of ∼390 $\mu A/cm^2$ at an applied field of 5.5 V/μm. Moreover, the turn-on field (E_{on}) of β-TiO_2/Si (i.e., 3.9 V/μm) and MoS_2/Si (i.e., 4.3 V/μm) emitters essential for gaining emission current density of 10 $\mu A/cm^2$ has been reduced considerably through coating with MoS_2 layers of various

DOI: 10.1021/acsomega.7b00345
ACS Omega 2017, 2, 2925−2934

thicknesses over β-TiO_2 nanorods. The E_{on} of 2.9, 3.1, and 2.5 V/μm was observed for ~40, ~20, and ~4 nm thick MoS_2 layers/shell, respectively. Similarly, threshold field (E_{thr}) of β-TiO_2/Si emitters (i.e., 4.8 V/μm) corresponding to the current density of 100 μA/cm^2 has been reduced to 3.6, 4.2, and 4.1 V/μm for respective thickness. The ~4 nm thick MoS_2 shell on β-TiO_2 nanorods gives the lowest values of E_{on} (i.e., 2.5 V/μm for current density of 10 μA/cm^2) compared with anatase and rutile phases of various 1D TiO_2 nanostructures such as nanotip, nanotubes, nanorods, nanowires, nanoneedles, nanoflowers, and 3D microspheres.[7,12,46,47] In addition, the formation of nanometric layers of MoS_2 over β-TiO_2 nanorods provided lower E_{on} compared with pure MoS_2 thin films in the form of protrusions (i.e., 2.8 V/μm)[48] and sheets (3.5 V/μm)[19] on Si substrate. Furthermore, our results show much lower values of E_{on} than those reported for carbon-doped (i.e., 21.9−5.0 V/μm),[14] Fe-doped (i.e., 12 V/μm),[13] and N-doped (i.e., 10, 9.21, and 6.54 V/μm) anatase TiO_2 nanotubes[6] and the composites of MoS_2@TiO_2[23,24] and MoS_2@SnO_2.[21] Moreover, these MoS_2/β-TiO_2/Si emitters appear to be better than the MoS_2@TiO_2 heterostructure array delivering E_{on} of 11 V/μm at a current density of 10 μA/cm^2[24] and hierarchical MoS_2@SnO_2 hetero-nanoflowers delivering E_{on} of 3.4 V/μm at a very low current density of 1 μA/cm^2.[21] However, turn-on fields of 2.2 and 2.5 V/μm were observed for the composite of MoS_2 layers heavily loaded over rutile TiO_2 hierarchical spheres of diameter >2.5 μm and rutile TiO_2 nanoparticles heavily enclosed over p-type MoS_2 flowerlike spheres of diameter 2 μm.[23] However, one cannot neglect that these lower values of turn-on field were defined at a current density of 1 μA/cm^2. Therefore, present 1D β-TiO_2 nanorods coated with ~4 nm 2D MoS_2 were found to be more efficient for providing low E_{on} of 2.5 V/μm at a relatively larger current density of 10 μA/cm^2 and also in the quest of field shielding effect because of their distinct morphological features. These observations are tabulated (Table ST2) for better presentation of the novelty of the present work.

A modified Fowler−Nordheim (F−N) equation mentioned below is applied to express the electric field-dependent variation in the emission current density of semiconducting nanostructures

$$J = \alpha_f a \Phi^{-1} E^2 \beta_{FE}^{\ 2} \exp\left(-\frac{b\Phi^{3/2}}{\beta_{FE} E}\nu_F\right) \quad (1)$$

where J is the device average FE current density, α_f is a macroscopic pre-exponential correction factor, a and b are constants ($a = 1.54 \times 10^{-6}$ A eV/V^2, $b = 6.83089 \times 10^3$ eV$^{-3/2}$ V/μm), Φ is the work function of the emitter, E is the applied average electric field, β_{FE} is the local electric field enhancement factor, and ν_F is a particular value of the principal Schottky−Nordheim barrier function ν (correction factor). The emission surface is treated to be rough for the MoS_2/β-TiO_2/Si emitters. Therefore, the ratio of both applied and local electric fields, which differ from each other at emission sites, is identified as the field enhancement factor (β_{FE}). A graph of $\ln\{J/E^2\}$ versus $(1/E)$, known as F−N plot, is further explained from eq 1. Therefore, the field enhancement factor (β_{FE}) is determined by the following equation

$$\beta_{FE} = \frac{-sb\Phi^{3/2}}{S} \quad (2)$$

where s (=0.95) is the value of the slope correction factor for the Schottky−Nordheim barrier. However, we considered $s = 1$, approximately, for simplicity.

The F−N plots for MoS_2-controlled MoS_2/β-TiO_2/Si emitters are shown in Figure 4b. The F−N plots are well resolved into two distinct sections. The distinct separations of F−N plots corroborate the well-defined band alignment of MoS_2 and β-TiO_2 after their layer/shell formation over other. The MoS_2 layer/shell over β-TiO_2 nanorods has tailored the values of β_{FE}. The β_{FE} values of 1687, 680, and 1209 and 2465, 1398, and 6331 are estimated for low-field region and high-field region, respectively, observed in MoS_2/β-TiO_2/Si emitters coated with ~40, ~20, and ~4 nm thick layers of MoS_2, respectively. The values of β_{FE} for MoS_2/β-TiO_2/Si emitters are higher than the values obtained for anatase and rutile phase of pure TiO_2 nanorods and nanotubes,[23,47] nanoparticle-decorated TiO_2 nanotubes,[7] Fe- and N-doped TiO_2 nanotubes,[6,13] MoS_2@TiO_2 heterostructures,[24] MoS_2@SnO_2 hetero-nanoflowers,[21] nano-heterojunctions of ZnO nanoparticles, and MoS_2 layers over rutile TiO_2 nanorods.[20,23] Nevertheless, the orthodoxy test utilizing spreadsheet provided by Forbes in ref 49 was performed to verify the feasibility of the FE measurements of MoS_2/β-TiO_2/Si emitters, especially, field enhancement factor (β_{FE}). The scaled-barrier-field (f) values evaluated for MoS_2/β-TiO_2/Si emitters coated with ~40, ~20, and ~4 nm thick layers of MoS_2 are given in Table 1.

Table 1. Scaled-Barrier-Field (f) Values Evaluated from F−N Plots for β-TiO_2 and MoS_2/β-TiO_2/Si Emitters Using Spreadsheet Provided in Ref 49[a]

material	f_{low}	f_{high}	orthodoxy test result	remarks
1D β-TiO_2 nanorods	0.30	0.49	pass	one highest-field point excluded
40 (±3) nm 2D MoS_2 layers	0.21	0.32	pass	
4 (±2) nm MoS_2@ 1D β-TiO_2	0.31	0.71*	apparently reasonable	three highest-field points excluded
20 (±3) nm MoS_2@ 1D β-TiO_2	0.29	0.61*	apparently reasonable	
40 (±3) nm MoS_2@ 1D β-TiO_2	0.27	0.58*	apparently reasonable	

[a]Single asterisk on f_{high} values indicates the apparently reasonable values (i.e., $f_{high} < 0.75$).

The emission situation is orthodox in all β-TiO_2/Si, MoS_2/Si, and MoS_2/β-TiO_2/Si emitters on the lower (f_{low}) and higher (f_{high}) scaled-barrier-field values. Although f_{high} values for MoS_2/β-TiO_2/Si emitters demonstrate an apparently reasonable emission condition, they are reduced considerably with an increase in the thickness of MoS_2 overlayer. Controlled loading of MoS_2 over 1D β-TiO_2 nanorods and well-defined band alignment between them might have resulted in the enhancement in FE with larger values of β_{FE} and lower E_{on} for MoS_2/β-TiO_2/Si emitters. Also, the appearance of the sharp morphological feature of highly conducting MoS_2 layers after coating on the top of nanorods assists in enhancing the local electric field of MoS_2/β-TiO_2/Si emitters. Moreover, morphological features of β-TiO_2 nanorods, such as individual dispersion, vertical alignment, and uniform separation, were maintained after coating ~4 nm thick layer/shell of MoS_2, which emerged as improved values of β_{FE} and low E_{on}. Coating of ~4 nm thick layer of MoS_2 along the β-TiO_2 nanorods

DOI: 10.1021/acsomega.7b00345
ACS Omega 2017, 2, 2925−2934

enhances the conductivity, and most of the injected electrons are transported easily toward the emission sites. This reduces the voltage drop along the nanorods and enhances the effective field at their tips, which leads to the observed enhancement of FE.

This phenomenon can be further elaborated by the band alignment of MoS_2/TiO_2 shown in Figure 5. The shell material

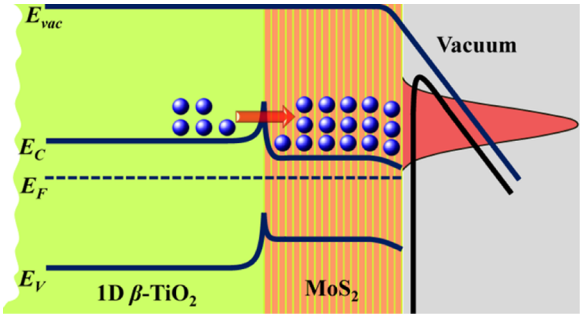

Figure 5. Schematic band alignment of MoS_2-decorated 1D β-TiO_2 nanorods.

with lower work function than that of the core material is well considered for the enhancement of FE. The work function of MoS_2 and TiO_2 is 4.0 and 4.3 eV,[19,47] respectively. Therefore, enhancement in the FE with better values of β and lower E_{on} for the MoS_2@β-TiO_2 was expected than that of pure β-TiO_2 nanorods and pristine 2D MoS_2 layer. The formation of this n−n junction at the interface of MoS_2 and β-TiO_2 leads to the favorable band alignment, which can be confirmed by two distinct sections of F−N plots of MoS_2/β-TiO_2/Si emitters. This well-defined band alignment favors tunneling and transportation of electrons from the conduction band of TiO_2 to the conduction band of MoS_2. In the case of β-TiO_2/Si emitters, at an applied electric field, the electrons from the conduction band or the state nearest to it contribute for FE. However, in MoS_2/β-TiO_2/Si emitters, the lower band gap of MoS_2 by 1.36 eV than that of TiO_2[50,51] provides relatively large number of electrons, which were endorsed by electrons tunneled from the conduction band of TiO_2. Consequently, the density of states dramatically increases and a significant number of electrons from MoS_2 layer/shell contribute to the FE. This is the reason why the improvement in the E_{on} was observed for the MoS_2/β-TiO_2/Si emitters than both pristine 2D MoS_2 and 1D β-TiO_2 nanorods. However, despite large E_{on} of MoS_2 (i.e., 4.3 V/μm), electron emission is relatively hampered for loading 40 and 20 nm thick layers of MoS_2 over β-TiO_2 than that for 4 nm thick layers. Enhancement in E_{on} has been observed after loading 4 nm thick MoS_2 layer over β-TiO_2 nanorods. Thus, the relatively lower band gap of MoS_2, very thin layer of MoS_2 over 1D nanorods, 1D morphology of β-TiO_2 nanorods, and well-defined band alignment collectively contribute to the enhancement of FE of MoS_2/β-TiO_2/Si emitters.

A stable FE current is one of the prerequisites for a possible development of field emitters in a variety of technological applications. Figure 6 shows the FE stability of MoS_2/β-TiO_2/Si emitters and the inset shows the FE image. The emission current (I) recorded at a preset current value of 1 μA showed no obvious degradation for continuous emission up to 180 min (t). Even though the β-TiO_2/Si emitters exhibit good stability (with slight current fluctuations of ±15% for average current

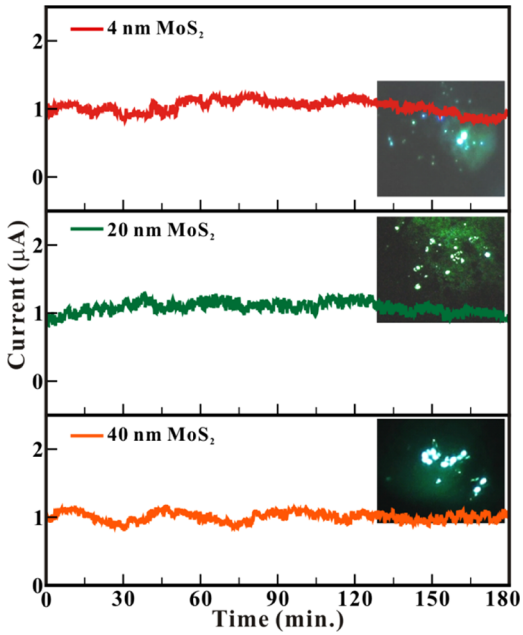

Figure 6. Field emission current stability (I−t) plot of 2D MoS_2@1D β-TiO_2 nanorods decorated with 40 nm (lower panel), 20 nm (middle panel), and 4 nm (upper panel) layer/shell of MoS_2.

values),[12] MoS_2/β-TiO_2/Si emitters rendered comparatively smaller current fluctuations (±10% for average current values) than that of pure β-TiO_2 nanorods, which confirms the improvement in their stability. Moreover, MoS_2/β-TiO_2/Si emitters composed of ∼4 nm MoS_2 layer are found to be more stable. The ∼4 nm thick MoS_2 layer/shell upholds the nanorods' morphology of β-TiO_2, which serve as emitters in large numbers, perhaps causing an improvement in the emission quality.

CONCLUSIONS

In conclusion, the large-area arrays of vertically aligned β-TiO_2 nanorods on Si substrate were coated with MoS_2 layer/shell utilizing PLD. The XPS analysis confirmed the formation of pure stoichiometric MoS_2 (i.e., Mo/S = 1:2.04) layers over the stoichiometric β-TiO_2 nanorods (i.e., Ti/O = 1:1.98). The turn-on field (at a current density of 10 μA/cm^2) of 3.9 and 4.3 V/μm exhibited by pristine β-TiO_2 nanorods and pure MoS_2, respectively, was considerably reduced further to 2.5 V/μm by coating 4 (±2) nm thick layer of MoS_2 over β-TiO_2 nanorods. However, morphological features of β-TiO_2 nanorods, that is, uniform separation, individual dispersion, and vertical alignment, and so on lead to acquiring low turn-on field and better FE characteristics. The ∼4 (±2) nm overlayer of conducting MoS_2 along the β-TiO_2 nanorods induces most of the injected electrons to transport easily toward emission sites, which is responsible for the further enhancement in FE behavior. The heteroarchitecture of MoS_2-coated β-TiO_2 nanorods holds the potential for applications in FE-based nanoelectronic devices, such as FE flat-panel displays and intense point electron sources in electron microscopes. Moreover, the present strategy employed to enhance the FE behavior via rational design of heteroarchitecture structure can be extended to improve the functionalities of various nanomaterials.

DOI: 10.1021/acsomega.7b00345
ACS Omega 2017, 2, 2925−2934

EXPERIMENTAL DETAILS

Large-area arrays of TiO_2 nanorods were synthesized on Si substrate utilizing HF-MVD technique. The details of the condensation of hot titanium vapor onto 1D brookite (β) TiO_2 nanorods are discussed in ref 12. Afterward, the 1D β-TiO_2 nanorods arrays were subjected to the formation of heteroarchitectures in combination with two-dimensional (2D) MoS_2 layers. The MoS_2 layers of various thicknesses were deposited on 1D β-TiO_2 nanorods utilizing PLD technique. The pellet of commercial MoS_2 powder sintered under argon (Ar) atmosphere at 900 °C for 12 h was mounted on a rotating target holder, which is fixed at a distance of ∼5 cm from the substrate holder inside the vacuum chamber. The large-area array of TiO_2 nanorods synthesized on Si substrate (i.e., TiO_2/Si) utilizing HF-MVD was mounted on the substrate holder facing the MoS_2 target. Once the pressure of the vacuum chamber was pumped down to $\sim 1 \times 10^{-4}$ mbar, the temperature of the TiO_2/Si-mounted substrate holder was maintained at ∼450 °C and the MoS_2 layers of various thicknesses were deposited on TiO_2 nanorods utilizing pulsed krypton−fluoride (KrF) excimer laser of wavelength (λ) 248 nm with 20 ns pulse at repetition rate of 5 Hz/s and energy density of 1 J/cm^2. The MoS_2 layer of various thicknesses such as 40 (±3), 20 (±3), and 4 (±2) nm was synthesized on TiO_2 nanorods by performing the deposition for various optimized time durations. After that, the surface morphology of the large-area arrays of MoS_2 coated β-TiO_2 nanorods was characterized using a field emission scanning electron microscope (FESEM, JEOL JSM-6500F). The chemical states of MoS_2-coated β-TiO_2 nanorods were analyzed using X-ray photoelectron spectrometer (XPS, Thermo Scientific Inc. K-α) with a microfocus monochromated Al Kα X-ray. The FE studies of MoS_2-coated TiO_2 nanorods were carried out in a vacuum chamber at a base pressure of $\sim 7.5 \times 10^{-9}$ Torr. The semi-transparent phosphor screen as an anode was maintained at an optimized distance of 2000 μm from the specimen/samples of MoS_2-coated β-TiO_2 nanorods (i.e., MoS_2/β-TiO_2/Si emitters). Further, to avoid the effect of contamination and loosely bound MoS_2 layers/protrusion, preconditioning of the samples was carried out by applying a voltage of ∼3 kV for 30 min. The FE current (I) was measured with an electrometer (Keithley 6514) at direct current (dc) voltage (V) applied using high-voltage dc power supply (0−40 kV, Spellman). The long-term stability of the FE current was recorded for the MoS_2/β-TiO_2/Si emitters consisting of 40, 20, and 4 nm thick layer of MoS_2.

ASSOCIATED CONTENT

Supporting Information

The Supporting Information is available free of charge on the ACS Publications website at DOI: 10.1021/acsomega.7b00345.

(A) Pure 2D MoS_2 layers and 2D MoS_2@1D β-TiO_2 nanorods; (B) Raman analysis of MoS_2@TiO_2; (C) XPS analysis; (D) field emission of pure 2D MoS_2 (Figures S1−S5; Tables ST1 and ST2) (PDF)

AUTHOR INFORMATION

Corresponding Author

*E-mail: rupesh@iiti.ac.in, devan_rs@yahoo.co.in.

ORCID

Rupesh S. Devan: 0000-0001-9550-7506

Author Contributions

RSD* conceived idea, designed experiments, and characterized all samples. RSD*, VPT, and VVA prepared the samples. RSD*, MAM, RTK, and PRC fabricated the device and performed field emission studies. RSD* analyzed the data and produced the results. RSD* wrote the manuscript in consultation with RSD, YRM, MAM, SIP, and LSM.

Funding

Department of Science and Technology (DST), Ministry of Science and Technology of India, for INSPIRE Faculty Award No. DST/INSPIRE Faculty Award/2013/IFA13-PH-63.

Notes

The authors declare no competing financial interest.

ACKNOWLEDGMENTS

The authors would like to thank the Department of Science and Technology (DST), Ministry of Science and Technology of India, for INSPIRE Faculty Award No. DST/INSPIRE Faculty Award/2013/IFA13-PH-63 for their financial support of this research. Authors are also thankful to Prof. Satishchandra B. Ogale, Department of Physics and Center for Energy Science, IISER Pune, India, for providing his research facilities and expertise on this manuscript.

REFERENCES

(1) Devan, R. S.; Patil, R. A.; Lin, J. H.; Ma, Y. R. One-dimensional Metal-Oxide Nanostructures: Recent Developments in Synthesis, Characterization, and Applications. *Adv. Funct. Mater.* **2012**, *22*, 3326−3370.

(2) Patil, R. A.; Devan, R. S.; Liou, Y.; Ma, Y.-R. Efficient Electrochromic Smart Windows of One-Dimensional Pure Brookite TiO_2 Nanoneedles. *Sol. Energy Mater. Sol. Cells* **2016**, *147*, 240−245.

(3) Devan, R. S.; Ma, Y.-R.; Patil, R. A.; Lukas, S.-M. Highly Stable Supercapacitive Performance of One-Dimensional (1D) Brookite TiO_2 Nanoneedles. *RSC Adv.* **2016**, *6*, 62218−62225.

(4) Kavan, L.; Kalbac, M.; Zukalova, M.; Exnar, I.; Lorenzen, V.; Nesper, R.; Graetzel, M. Lithium Storage in Nanostructured TiO_2 made by Hydrothermal Growth. *Chem. Mater.* **2004**, *16*, 477−485.

(5) Alivov, Y.; Klopfer, M.; Molloi, S. Effect of TiO_2 Nanotube Parameters on Field Emission Properties. *Nanotechnology* **2010**, *21*, No. 505706.

(6) Antony, R. P.; Mathews, T.; Panda, K.; Sundaravel, B.; Dash, S.; Tyagi, A. K. Enhanced Field Emission Properties of Electrochemically Synthesized Self-Aligned Nitrogen-Doped TiO_2 Nanotube Array Thin Films. *J. Phys. Chem. C* **2012**, *116*, 16740−16746.

(7) Xu, X.; Tang, C. C.; Zeng, H. B.; Zhai, T. Y.; Zhang, S. Q.; Zhao, H. J.; Bando, Y.; Golberg, D. Structural Transformation, Photocatalytic, and Field-Emission Properties of Ridged TiO_2 Nanotubes. *ACS Appl. Mater. Interfaces* **2011**, *3*, 1352−1358.

(8) Liang, J.; Zhang, G. M. TiO_2 Nanotip Arrays: Anodic Fabrication and Field-Emission Properties. *ACS Appl. Mater. Interfaces* **2012**, *4*, 6053−6061.

(9) Wu, J. M.; Shih, H. C.; Wu, W. T. Electron Field Emission From Single Crystalline TiO_2 Nanowires Prepared by Thermal Evaporation. *Chem. Phys. Lett.* **2005**, *413*, 490−494.

(10) Wang, C. W.; Chen, J. B.; Wang, L. Q.; Kang, Y. M.; Li, D. S.; Zhou, F. Single Crystal TiO_2 Nanorods: Large-scale Synthesis and Field Emission. *Thin Solid Films* **2012**, *520*, 5036−5041.

(11) Kandiel, T. A.; Feldhoff, A.; Robben, L.; Dillert, R.; Bahnemann, D. W. Tailored Titanium Dioxide Nanomaterials: Anatase Nanoparticles and Brookite Nanorods as Highly Active Photocatalysts. *Chem. Mater.* **2010**, *22*, 2050−2060.

(12) Devan, R. S.; Ma, Y.-R.; More, M. A.; Khare, R. T.; Antad, V. V.; Patil, R. A.; Thakare, V.; Dhayal, R. S.; Schmidt-Mende, L. Promising Field Electron Emission Performance of Vertically Aligned One-

DOI: 10.1021/acsomega.7b00345
ACS Omega 2017, 2, 2925−2934

dimensional (1D) Brookite (β) TiO_2 Nanorods. *RSC Adv.* **2016**, *6*, 98722−98729.
(13) Wang, C. C.; Wang, K. W.; Perng, T. P. Electron Field Emission From Fe-doped TiO_2 Nanotubes. *Appl. Phys. Lett.* **2010**, *96*, No. 143102.
(14) Wang, L. Q.; Wang, C. W.; Chen, J. B.; Guo, R. S.; Zhou, F.; Liu, W. M. Electron Field Emission From the Carbon-doped TiO_2 nanotube Arrays. *Thin Solid Films* **2011**, *519*, 8173−8177.
(15) Ho, W.; Yu, J. C.; Lin, J.; Yu, J. G.; Li, P. S. Preparation and Photocatalytic Behavior of MoS_2 and WS_2 Nanocluster Sensitized TiO_2. *Langmuir* **2004**, *20*, 5865−5869.
(16) Zhou, W.; Yin, Z. Y.; Du, Y. P.; Huang, X.; Zeng, Z. Y.; Fan, Z. X.; Liu, H.; Wang, J. Y.; Zhang, H. Synthesis of Few-Layer MoS_2 Nanosheet-Coated TiO_2 Nanobelt Heterostructures for Enhanced Photocatalytic Activities. *Small* **2013**, *9*, 140−147.
(17) Villevieille, C.; Wang, X.-J.; Krumeich, F.; Nesper, R.; Novák, P. MoS2 coating on MoO_3 nanobelts: A Novel Approach for a High Specific Charge Electrode for Rechargeable Li-ion Batteries. *J. Power Sources* **2015**, *279*, 636−644.
(18) Mak, K. F.; Lee, C.; Hone, J.; Shan, J.; Heinz, T. F. Atomically Thin MoS_2: A New Direct-Gap Semiconductor. *Phys. Rev. Lett.* **2010**, *105*, No. 136805.
(19) Kashid, R. V.; Late, D. J.; Chou, S. S.; Huang, Y. K.; De, M.; Joag, D. S.; More, M. A.; Dravid, V. P. Enhanced Field-Emission Behavior of Layered MoS_2 Sheets. *Small* **2013**, *9*, 2730−2734.
(20) Tan, Y. H.; Yu, K.; Li, J. Z.; Fu, H.; Zhu, Z. Q. MoS_2@ZnO Nano-Heterojunctions With Enhanced Photocatalysis and Field Emission Properties. *J. Appl. Phys.* **2014**, *116*, No. 064305.
(21) Li, J.; Yu, K.; Tan, Y.; Fu, H.; Zhang, Q.; Cong, W.; Song, C.; Yin, H.; Zhu, Z. Facile Synthesis of Novel MoS_2@SnO_2 Heteronanoflowers and Enhanced Photocatalysis and Field-emission Properties. *Dalton Trans.* **2014**, *43*, 13136−13144.
(22) Huo, K. F.; Zhang, X. M.; Hu, L. S.; Sun, X. J.; Fu, J. J.; Chu, P. K. One-Step Growth and Field Emission Properties of Quasialigned TiO_2 Nanowire/Carbon Nanocone Core-Shell Nanostructure Arrays on Ti Substrates. *Appl. Phys. Lett.* **2008**, *93*, No. 013105.
(23) Fu, H.; Yu, K.; Li, H. L.; Li, J. Z.; Guo, B. J.; Tan, Y. H.; Song, C. Q.; Zhu, Z. Q. Enhanced Field Emission and Photocatalytic Performance of MoS_2 Titania Nanoheterojunctions via Two Synthetic Approaches. *Dalton Trans.* **2015**, *44*, 1664−1672.
(24) Yang, J.; Liang, J.; Zhang, G. M.; Li, J.; Liu, H.; Shen, Z. Y. Heterostructures of MoS_2 Nanofilms on TiO_2 Nanorods Used as Field Emitters. *Vacuum* **2016**, *123*, 17−22.
(25) Devan, R. S.; Gao, S. Y.; Ho, W. D.; Lin, J. H.; Ma, Y. R.; Patil, P. S.; Liou, Y. Electrochromic Properties of Large-Area and High-Density Arrays of Transparent One-Dimensional β-Ta_2O_5 Nanorods on Indium-Tin-Oxide Thin-Films. *Appl. Phys. Lett.* **2011**, *98*, No. 133117.
(26) Devan, R. S.; Ho, W. D.; Lin, J. H.; Wu, S. Y.; Ma, Y. R.; Lee, P. C.; Liou, Y. X-ray Diffraction Study of a Large-Scale and High-Density Array of One-Dimensional Crystalline Tantalum Pentoxide Nanorods. *Cryst. Growth Des.* **2008**, *8*, 4465−4468.
(27) Devan, R. S.; Ho, W. D.; Wu, S. Y.; Ma, Y. R. Low-Temperature Phase Transformation and Phonon Confinement in One-Dimensional Ta_2O_5 Nanorods. *J. Appl. Crystallogr.* **2010**, *43*, 498−503.
(28) Lin, J. H.; Patil, R. A.; Wu, M. A.; Yu, L. G.; Liu, K. D.; Gao, W. T.; Devan, R. S.; Ho, C. H.; Liou, Y.; Ma, Y. R. Large-Area Nanoscale Farmland-Like Surfaces of One-Dimensional NbO_2 Nanorods With Multi-Growth Directions: Studies on the Purple-Blue Photoluminescence and Low-Field Electron Emissions. *J. Mater. Chem. C* **2014**, *2*, 8667−8672.
(29) Devan, R. S.; Lin, C. L.; Gao, S. Y.; Cheng, C. L.; Liou, Y.; Ma, Y. R. Enhancement of Green-Light Photoluminescence of Ta_2O_5 Nanoblock Stacks. *Phys. Chem. Chem. Phys.* **2011**, *13*, 13441−13446.
(30) Patil, R. A.; Devan, R. S.; Lin, J. H.; Liou, Y.; Ma, Y. R. An Efficient Methodology for Measurement of the Average Electrical Properties of Single One-Dimensional NiO Nanorods. *Sci. Rep.* **2013**, *3*, No. 3070.
(31) Yao, J.; Zheng, Z. Q.; Yang, G. W. Promoting the Performance of Layered-Material Photodetectors by Alloy Engineering. *ACS Appl. Mater. Interfaces* **2016**, *8*, 12915−12924.
(32) Yao, J. D.; Zheng, Z. Q.; Shao, J. M.; Yang, G. W. Stable, highly-responsive and broadband photodetection based on large-area multilayered WS_2 films grown by pulsed-laser deposition. *Nanoscale* **2015**, *7*, 14974−14981.
(33) Willmott, P. R.; Huber, J. R. Pulsed laser vaporization and deposition. *Rev. Mod. Phys.* **2000**, *72*, 315−328.
(34) Serna, M. I.; Yoo, S. H.; Moreno, S.; Xi, Y.; Oviedo, J. P.; Choi, H. J.; Alshareef, H. N.; Kim, M. J.; Minary-Jolandan, M.; Quevedo-Lopez, M. A. Large-Area Deposition of MoS_2 by Pulsed Laser Deposition with In Situ Thickness Control. *ACS Nano* **2016**, *10*, 6054−6061.
(35) Splendiani, A.; Sun, L.; Zhang, Y. B.; Li, T. S.; Kim, J.; Chim, C. Y.; Galli, G.; Wang, F. Emerging Photoluminescence in Monolayer MoS_2. *Nano Lett.* **2010**, *10*, 1271−1275.
(36) Wang, Y.; Sun, H. J.; Tan, S. J.; Feng, H.; Cheng, Z. W.; Zhao, J.; Zhao, A. D.; Wang, B.; Luo, Y.; Yang, J. L.; Hou, J. G. Role of Point Defects on the Reactivity of Reconstructed Anatase Titanium Dioxide (001) Surface. *Nat. Commun.* **2013**, *4*, No. 2214.
(37) Patil, R. A.; Devan, R. S.; Lin, J. H.; Ma, Y. R.; Patil, P. S.; Liou, Y. Efficient Electrochromic Properties of High-Density and Large-Area Arrays of One-Dimensional NiO Nanorods. *Sol. Energy Mater. Sol. Cells* **2013**, *112*, 91−96.
(38) Devan, R. S.; Lin, J. H.; Ho, W. D.; Wu, S. Y.; Liou, Y.; Ma, Y. R. Investigation of High-Temperature Phase Transformation in One-Dimensional Ta_2O_5 Nanorods. *J. Appl. Crystallogr.* **2010**, *43*, 1062−1067.
(39) Devan, R. S.; Ho, W. D.; Chen, C. H.; Shiu, H. W.; Ho, C. H.; Cheng, C. L.; Wu, S. Y.; Liou, Y.; Ma, Y. R. High Room-Temperature Photoluminescence of One-Dimensional Ta_2O_5 Nanorod Arrays. *Nanotechnology* **2009**, *20*, No. 445708.
(40) Weber, T.; Muijsers, J. C.; vanWolput, H.; Verhagen, C. P. J.; Niemantsverdriet, J. W. Basic reaction Steps in the Sulfidation of Crystalline MoO_3 to MoS_2 as Studied by X-ray Photoelectron and Infrared Emission Spectroscopy. *J. Phys. Chem.* **1996**, *100*, 14144−14150.
(41) Liu, H.; Lv, T.; Zhu, C. K.; Su, X.; Zhu, Z. F. Efficient Synthesis of MoS_2 Nanoparticles Modified TiO_2 Nanobelts With Enhanced Visible-Light-Driven Photocatalytic Activity. *J. Mol. Catal. A: Chem.* **2015**, *396*, 136−142.
(42) Lin, T. R.; Wang, J.; Guo, L. Q.; Fu, F. F. Fe_3O_4@MoS_2 Core-Shell Composites: Preparation, Characterization, and Catalytic Application. *J. Phys. Chem. C* **2015**, *119*, 13658−13664.
(43) Li, B. B.; Qiao, S. Z.; Zheng, X. R.; Yang, X. J.; Cui, Z. D.; Zhu, S. L.; Li, Z. Y.; Liang, Y. Q. Pd Coated MoS_2 Nanoflowers for Highly Efficient Hydrogen Evolution Reaction Under Irradiation. *J. Power Sources* **2015**, *284*, 68−76.
(44) Merki, D.; Fierro, S.; Vrubel, H.; Hu, X. L. Amorphous Molybdenum Sulfide Films as Catalysts for Electrochemical Hydrogen Production in Water. *Chem. Sci.* **2011**, *2*, 1262−1267.
(45) Ambrosi, A.; Sofer, Z.; Pumera, M. Lithium Intercalation Compound Dramatically Influences the Electrochemical Properties of Exfoliated MoS_2. *Small* **2015**, *11*, 605−612.
(46) Liu, B.; Aydil, E. S. Growth of Oriented Single-Crystalline Rutile TiO_2 Nanorods on Transparent Conducting Substrates for Dye-Sensitized Solar Cells. *J. Am. Chem. Soc.* **2009**, *131*, 3985−3990.
(47) Zhang, X. Q.; Chen, J. B.; Wang, C. W.; Liao, A. Z.; Su, X. F. Low-temperature Liquid Phase Reduced TiO_2 Nanotube Arrays: Synergy of Morphology Manipulation and Oxygen Vacancy Doping for Enhancement of Field Emission. *Nanotechnology* **2015**, *26*, No. 175705.
(48) Late, D. J.; Shaikh, P. A.; Khare, R.; Kashid, R. V.; Chaudhary, M.; More, M. A.; Ogale, S. B. Pulsed Laser-Deposited MoS_2 Thin Films on W and Si: Field Emission and Photoresponse Studies. *ACS Appl. Mater. Interfaces* **2014**, *6*, 15881−15888.

DOI: 10.1021/acsomega.7b00345
ACS Omega 2017, 2, 2925−2934

(49) Forbes, R. G. Development of a Simple Quantitative Test for Lack of Field Emission Orthodoxy. *Proc. R. Soc. A* **2013**, *469*, No. 20130271.
(50) King, L. A.; Zhao, W.; Chhowalla, M.; Riley, D. J.; Eda, G. Photoelectrochemical Properties of Chemically Exfoliated MoS_2. *J. Mater. Chem. A* **2013**, *1*, 8935−8941.
(51) Di Paola, A.; Bellardita, M.; Ceccato, R.; Palmisano, L.; Parrino, F. Highly Active Photocatalytic TiO_2 Powders Obtained by Thermohydrolysis of $TiCl_4$ in Water. *J. Phys. Chem. C* **2009**, *113*, 15166−15174.

DOI: 10.1021/acsomega.7b00345
ACS Omega 2017, 2, 2925−2934